ELSEVIER

The acceleration of charged nano-particles in gas stream of supersonic de-Laval-type nozzle coupled with static electric field

Tien-Chien Jen [a,*], Liangming Pan [a,b], Longjian Li [b], Qinghua Chen [a,b], Wenzhi Cui [b]

[a] *Department of Mechanical Engineering, University of Wisconsin, 3200 N. Cramer Street, P.O. Box 784, Milwaukee, WI 53211, United States*
[b] *College of Thermal Power Engineering, Chongqing University, Chongqing, PR China*

Abstract

This paper presents a numerical analysis of an innovative method for nano-scale particle deposition, called Electrostatic-force-assisted cold gas dynamic spray (ECGDS). The transport characteristics of nano-scale charged particles in supersonic gas stream coupled with electrostatic field are simulated. Outside the nozzle, there exists bow shock near the substrate, which causes steep pressure increase across the shock. When the gas flow penetrates the bow shock and approaches to the substrate, the carrier gas speed decreases to nearly zero. In this study, electrostatic force is used to assist the charged particle to achieve high velocity upon impact of the substrate. The effect of electrostatic field to the velocity distribution of charged particles is investigated. It is found that smaller particles have the higher impact velocities on substrate. The higher particle charge densities can lead to higher particle impact velocities; and the closer the particles approach to the substrate, the stronger the electrostatic forces act on particles. For nano-scale particles the particle density (i.e. different materials) almost has no influence on the velocity profile.
© 2005 Elsevier Ltd. All rights reserved.

Keywords: Electrostatic-force-assisted cold gas dynamic spray (ECGDS); Static electric potential; Bow shock; Charged nano-scale particle

1. Introduction

The abilities to deposit different materials such as insulators, semiconductors and metals on a nanometer scale are crucial in the design of future electronic and opto-electronic devices. Improvements on these techniques will open doors for the production of new devices, which cannot be produced with conventional methods. For instance, films of monodisperse SnO_2-particles can be used for sensor applications [1], closed lines of metal nano-particles such as Au or Ag or Cu may be used as nano-wires for the power supply of electronic devices, single nano-particles can be used for single elec-

tronic transistor applications [2], arrangements of single nano-particles might be used for data storage [3] or light emitting devices [4] or even new kinds of logic circuits [5], and Au nano-particles can be used as catalysts to allow selective growth of nano-whiskers [6]. In order to successfully produce the above-mentioned applications, it depends strongly on the abilities to deposit nano-particles on locally defined areas of a flat substrate surface.

Cold gas dynamic spray (CGDS) is an emerging technology for coating surfaces [7]. The spray process is based on the impact on and the subsequent adherence to a substrate of particles of high kinetic energy. Current CGDS involves injecting microscopic powdered particles of a metal or solid material into a supersonic jet of rapidly expanding gas and then shooting them at a target surface. The low temperature CGDS process has been considered as a promising alternate process to the well-established high temperature thermal spraying process

---

* Corresponding author. Tel.: +1 414 229 2307; fax: +1 414 229 6958.
  E-mail address: jen@cae.uwm.edu (T.-C. Jen).

Nomenclature

c_p	specific heat capacity (J/(kg K))
$C_{\varepsilon 1}$, $C_{\varepsilon 2}$, C_μ	turbulent model constants
C_D	drag coefficient
d_p	particle diameter (m)
E	electric field intensity (V/m)
F_D	drag force per unit particle mass (N/kg)
F_E	electric force (N/kg)
g	acceleration of gravity (m/s^2)
k	turbulent kinetic energy (m^2/s^2)
m_p	mass of the particle (kg)
p	pressure (N/m^2)
Pr	molecular Prandtl number
q_p	electrons on single particle
r	radial distance (m)
Re	Reynolds number
T	temperature (K)
t	time (s)
u_i	velocity component in i-direction ($i = 1, 2$) (m/s)
v_x	velocity of x direction (m s^{-1})
v_r	velocity of radial direction (m s^{-1})

v_z	the swirl velocity (m s^{-1})
x_i	Cartesian coordinate in the i-direction ($i = 1, 2$) (m)

Greek symbols

Γ	thermal conductivity (W/m K)
ε	dissipation ratio of turbulent kinetic energy (m^2/s^3)
μ	viscosity (kg/m s)
μ_{eff}	effective viscosity (kg/m s)
ρ	density of fluid (kg/m^3)
α_T, α_k, α_ε	inverse effective Prandtl number for energy equations, T, k and ε
Φ	electric potential, (V)

Subscripts

i, j, k	general spatial indices
eff	turbulent effective parameters
mol	molecule property
p	particle property
t	turbulent quantity

to avoid deleterious effects of high temperature oxidation, evaporation, melting, crystallization and thermal residual stresses. The advantages of this approach also include the high bond strength of the particle, the high production rate due to the high deposition rate (deposition efficiencies of up to 80%), and the ability to recycle the powders. In the CGDS process particles are accelerated by means of a carrier gas in a converging–diverging (de-Laval-type) supersonic nozzle. The interaction of the supersonic core flow of the jet with the substrate results in an inherently transonic flow field. This causes a bow shock formed right ahead of the substrate. Because of the rapid deceleration of particles through the bow shock current CGDS techniques can only treat the particle size ranges from 5 µm to 50 µm, which has large enough inertia momentum to overcome the bow shock. It has been shown in Jen et al. [8,9] that when the particle size falls below 100 nm, the particles cannot penetrate the shocks to reach the substrate.

In this study, an electrostatic force is used to assist the particles when they are passing through the shock. This approach, in fact, is to couple electrostatic force with the supersonic gas-particle two-phase flow. The purpose of this approach is to supply nano-particles with sufficient momentums to pass through the bow shock and deposit on the substrate with sufficient impact velocity. This innovative method for nano-scale particle deposition is called as electrostatic-force-assisted cold

gas dynamic spray (ECGDS) technique. Although a few works have been done on the simulation of CGDS particle behaviours inside and outside de-Laval nozzle, the transport characteristics of nano-scale charged particles in supersonic gas stream coupled with electrostatic field are still in an unexploratory territory, in particular for the study of the interaction of nano-scale charged particles under the action of electrostatic field with the shocks outside supersonic nozzle. In this paper, comprehensive numerical simulations are reported for the acceleration of particles in a supersonic nitrogen stream with the aide of the electrostatic force. The effects of particle size, charge density, and particle density were investigated in this study. This study also investigated the influence of charge density upon the velocity distribution of the particles.

2. Mathematical models

The positively charged particle flow inside and outside the de-Laval-type nozzle of the ECGDS system is schematically shown in Fig. 1. The substrate is connected to a high voltage generator to establish a negative potential around it. The carrier gas enters the nozzle to carry positively charged particles from the particle-feed pipe at the inlet of the convergent section. For this physical model, the following assumptions were made to sim-
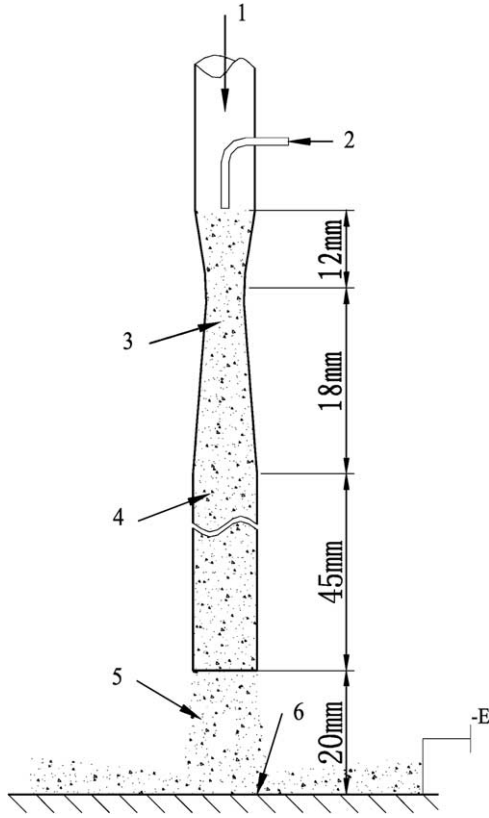
Fig. 1. Schematic configuration of electrostatic-force-assisted cold gas dynamic spraying: (1) inlet of high pressure carrier gas, (2) inlet of charged metal particles with a positive charge, (3) de-Laval-type nozzle with a ratio of expansion of $A_E/A_* = 28.4$, (4) tube for particle acceleration, (5) high-speed carrier gas with particles, and (6) substrate with a negative voltage.

plify the formulation without compromising the essential features. They are:

(1) Two-dimensional axis-symmetric geometry;
(2) Dilute spray condition (no interactions between particles as well as between particles and the continuous phase.);
(3) The effect of the presence of the space charge density is negligible because of the dilute particles condition in the gas stream.

2.1. Governing equations for the continuous phase of carrier gas

For a two-dimensional axis-symmetric geometry, the continuity equation is given by

$$\frac{\partial}{\partial x}(\rho v_x) + \frac{\partial}{\partial r}(\rho v_r) + \frac{\rho v_r}{r} = 0 \tag{1}$$

Conservation of momentum for an inertial reference frame is described by [11]. The axial and radial momentum conservation equations are given by

$$\frac{\partial}{\partial x}(r\rho v_x v_x) + \frac{\partial}{\partial r}(r\rho v_r v_x) = -r\frac{\partial p}{\partial x}$$
$$+ \frac{\partial}{\partial x}\left[r\mu_{\text{eff}}\left(2\frac{\partial v_x}{\partial x} - \frac{2}{3}(\nabla \cdot \vec{v})\right)\right]$$
$$+ \frac{\partial}{\partial r}\left[r\mu_{\text{eff}}\left(\frac{\partial v_x}{\partial r} + \frac{\partial v_r}{\partial x}\right)\right] \tag{2}$$

and

$$\frac{\partial}{\partial x}(r\rho v_x v_r) + \frac{\partial}{\partial r}(r\rho v_r v_r) = -r\frac{\partial p}{\partial r}$$
$$+ \frac{\partial}{\partial x}\left[r\mu_{\text{eff}}\left(2\frac{\partial v_r}{\partial x} - \frac{2}{3}(\nabla \cdot \vec{v})\right)\right]$$
$$+ \frac{\partial}{\partial r}\left[r\mu_{\text{eff}}\left(\frac{\partial v_x}{\partial r} + \frac{\partial v_r}{\partial x}\right)\right]$$
$$- 2\mu_{\text{eff}}\frac{v_r}{r} + \frac{2}{3}\mu_{\text{eff}}(\nabla \cdot \vec{v}) + \rho v_z^2 \tag{3}$$

where

$$\nabla \cdot \vec{v} = \frac{\partial v_x}{\partial x} + \frac{\partial v_r}{\partial r} + \frac{v_r}{r} \tag{4}$$

and v_z is the swirl velocity.

The corresponding equation for conservation of energy can be written as

$$\frac{\partial}{\partial x_i}(\rho u_i c_p T) = \frac{\partial}{\partial x_i}\left[\alpha_T\left(\mu_{\text{eff}}\frac{\partial T}{\partial x_i}\right)\right]$$
$$+ \frac{\partial u_i}{\partial x_j}\left[\mu_{\text{eff}}\left(\frac{\partial u_i}{\partial x_j} + \frac{\partial u_j}{\partial x_i}\right) - \frac{2}{3}\frac{\partial u_k}{\partial x_k}\right] \tag{5}$$

Note that the loss of mechanical energy due to viscosity in compressible flow is accounted for in the above equation.

The turbulent kinetic energy and its dissipation rate are

$$\frac{\partial}{\partial x}(\rho k v_x) + \frac{\partial}{\partial r}(\rho k v_r) = \frac{\partial}{\partial x}\left(\alpha_k \mu_{\text{eff}}\frac{\partial k}{\partial x}\right) + \frac{\partial}{\partial r}\left(\alpha_k \mu_{\text{eff}}\frac{\partial k}{\partial r}\right)$$
$$+ G_k - \rho\varepsilon - Y_M \tag{6}$$

and

$$\frac{\partial}{\partial x}(\rho\varepsilon v_x) + \frac{\partial}{\partial r}(\rho\varepsilon v_r) = \frac{\partial}{\partial x}\left(\alpha_\varepsilon \mu_{\text{eff}}\frac{\partial\varepsilon}{\partial x}\right) + \frac{\partial}{\partial r}\left(\alpha_\varepsilon \mu_{\text{eff}}\frac{\partial\varepsilon}{\partial r}\right)$$
$$+ C_{1\varepsilon}\frac{\varepsilon}{k}G_k - C_{2\varepsilon}\rho\frac{\varepsilon^2}{k}$$
$$- \frac{C_\mu \rho\eta^3(1 - \eta/\eta_0)}{1 + \beta\eta^3}\frac{\varepsilon^2}{k} \tag{7}$$

In these equations, G_k represents the generation of turbulence kinetic energy due to mean velocity gradients, which can be calculated by

$$G_k = -\rho\overline{u_i'u_j'}\frac{\partial u_j}{\partial x_i} \tag{8}$$

The corresponding effective viscosity is defined as

$$\mu_{\text{eff}} = \mu + \mu_{\text{t}} \tag{9}$$

In a high-Reynolds-number range,

$$\mu_{\text{t}} = \rho C_\mu \frac{k^2}{\varepsilon} \tag{10}$$

Y_M represents the contribution of the fluctuating dilatation in compressible turbulence to the overall dissipation rate [10], and can be evaluated from

$$Y_M = 2\rho\varepsilon M_{\text{t}}^2 \tag{11}$$

Here M_{t} is the turbulent Mach number ($M_{\text{t}}^2 = 2k/a^2$) and a is the mean speed of sound.

The values of η can be computed from

$$\eta \equiv Sk/\varepsilon \tag{12}$$

with

$$S = \sqrt{2s_{ij}s_{ij}} \tag{13}$$

and

$$s_{ij} = \frac{\partial u_i}{\partial x_j} + \frac{\partial u_j}{\partial x_i} \tag{14}$$

The necessary coefficients for the RNG k–ε turbulence model are described in Table 1.

The method used for the simulation of particle phase is the discrete phase model (DPM). In this method, the discrete phase is solved by the Lagrangian approach. Particle trajectories are calculated by solving the equations of motion for particles

$$\frac{\text{d}u_{\text{p}}}{\text{d}t} = F_{\text{D}}(u - u_{\text{p}}) + F_{\text{G}} + F_{\text{E}} \tag{15}$$

where the drag force $F_{\text{D}}(u - u_{\text{p}})$ and the gravitational force F_{G} are defined in [11] as shown below

$$F_{\text{D}} = \frac{18\mu}{\rho_p d_{\text{p}}^2} \frac{C_D Re}{24} \tag{16}$$

$$F_{\text{G}} = \frac{g_x(\rho_{\text{p}} - \rho)}{\rho_{\text{p}}} \tag{17}$$

u_{p} is the particle velocity, u is the carrier gas velocity and F_{E} is the electrostatic force defined in next section.

2.2. The equation of electrostatic field and the electrostatic force

The electric field, which is generated by the applied voltage to the substrate can be described by Laplace equation [11]

$$\nabla^2 \Phi = 0 \tag{18}$$

where the potential Φ is related to the electric field intensity according to

$$E = -\nabla\Phi \tag{19}$$

The electric force F_{E} in Eq. (15) is defined as [11],

$$\vec{F}_{\text{E}} = q_{\text{p}}\vec{E} + \frac{q_{\text{p}}^2}{16\pi a^2} \tag{20}$$

where the first term on the right side is the Coulomb force and the second term is the image force, which gives a significant contribution to the electric force only when particles are in the vicinity of the target surface. Here, q_{p} is the particle charge and a is the spacing between the particle and the target surface.

2.3. Boundary conditions

On the substrate a fixed potential of $-80\,\text{kV}$ was imposed, which creates a large electrostatic force on charged particles in the vicinity of the substrate with the electric potential of the nozzle set to be zero.

For the fluid flow, the boundary conditions were gage inlet pressure of 1.90 MPa, inlet absolute temperature of 773 K, ambient gauge pressure of zero, and ambient absolute temperature of 350 K. For solid–fluid interface, no-slip and adiabatic conditions were assumed for momentum and energy equation, respectively.

2.4. Numerical computation

The governing equations for the compressible flows and particle motion inside and outside the nozzle are solved using a control-volume finite element method (CVFEM). The second-order upwinding scheme was selected for the discretization of the convection term in the
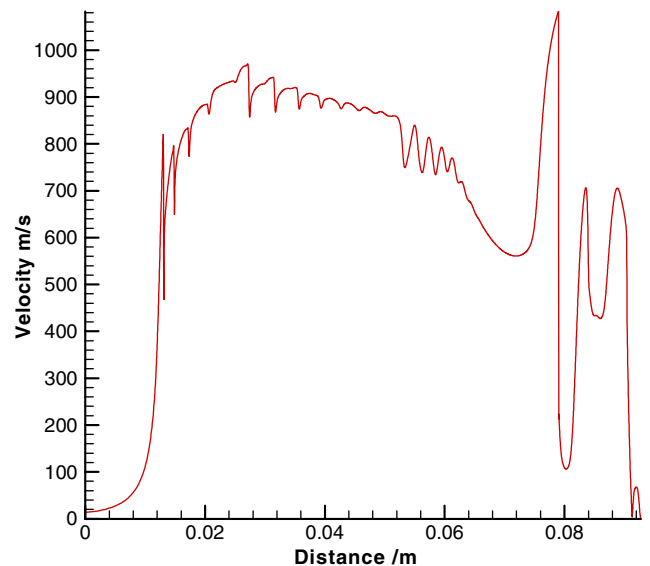

Fig. 2. Velocity magnitude of carrier gas along the axial of the nozzle.

Table 1
Values assigned to RNG k–ε turbulence model coefficients

C_μ	α_k	α_ε	α_T	$C_{\varepsilon 1}$	$C_{\varepsilon 2}$	η_0	β
0.0845	0.719	0.719	0.9	1.42	1.68	4.38	0.012

governing equations. A structured non-uniform grid system has been used to discretize the computation domain. For a compressible flow with weak shocks, the gradient adaption is used for the solution of the supersonic flow. The pressure gradients in the solution are used to adapt the grid. The calculations on the adapted grid result in a much sharper definition of the shocks. The grid independence was investigated in the analysis by adopting different grid distributions. The grid independence test indicated that the grid system of 500,000 is sufficient for a satisfactory solution.

Based on the assumption that the particle phase is present at a low mass and momentum loading, in which the continuous phase is not impacted by the presence of the discrete phase, the two different phases can then be uncoupled to solve iteratively. This is a two-step proce-

dure. First, the SIMPLE method is used to solve the continuous phase flow field. Then the particle trajectories for discrete phase of interest are calculated. In this paper, the flow media is nitrogen (N_2), the particle phases are carbon (C), copper (Cu) and platinum (Pt), respectively.

3. Results and discussion

Fig. 2 shows the velocity profile of carrier gas N_2 along the axis of the nozzle. The gas velocity reached a maximum at the exit of the divergent section. At the connection of the straight section after the divergent nozzle, the supersonic flow is tilted by a small angle toward the wall. This includes cone-shape weak shock
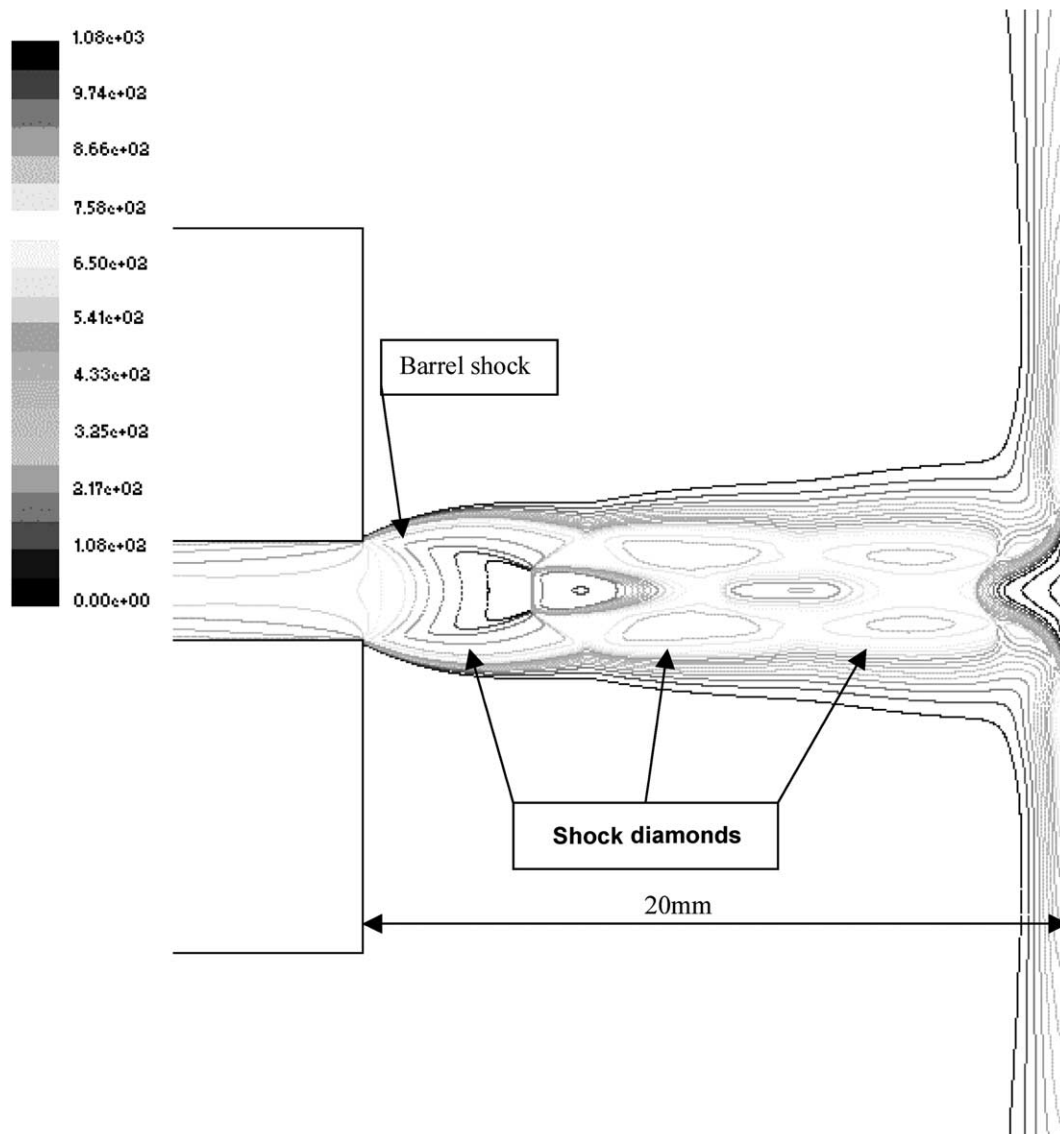

Fig. 3. The velocity contour of N_2 outside the nozzle.

waves, and the multiple reflections of the shock waves at the wall and nozzle center result in the velocity fluctuation at the centerline. The friction at the straight section causes the gas velocity to decrease significantly. After the nozzle exit, shock diamonds are formed due to the under-expansion of gas flow (Fig. 3). The adjustment of supersonic flow to the atmospheric pressure is through shock waves. Between the nozzle exit and the substrate, there exists a well-formed Mach disk located close to the nozzle exit, a subsequent second weaker Mach disk and a bow shock formed on the substrate can also be seen in Fig. 4. The contour plot shows that the low static pressure before Mach disk leads to rapid compression and deceleration of flow gas at the centerline. As the gas penetrates the Mach disk and high static pressure after the Mach disk immediately leads to rapid gas expansion and acceleration till it reaches the next oblique shock at the second shock disk. There is a steep pressure increase across the bow shock. Unlike the region following the Mach disk, the pressure in this region is well confined by the bow shock causing a much higher pressure increase at the substrate and generates a signifi-

cantly different flow pattern. The flow velocity decreases rapidly to nearly zero when it approaches the wall.

Fig. 5 shows the static electric potential distribution of the field. It can be seen that the maximum electric potential gradient is in the vicinity of substrate. This is favorable for this particular application since the electrostatic force used to assist the charged particles is the largest in this region, where the mach disk and bow shock appear.

Fig. 6 is the trace of carbon particles of four different diameters with of 1000 positive electron charges. It is shown that the effect of electrostatic force on the velocity distribution of carbon particles outside the nozzle is very significant. The smaller the particles are, the higher the impact velocities of particles can be achieved at the substrate. For the carbon particle diameter of 20 nm, the impact velocity is about 700 m/s; while the particle size increase to 500 nm, the impact velocity decreases to less than 50 m/s. It is worth noting that in conventional CGDS without the electrostatic field, large particles ($\geqslant 5 \mu m$) usually have significant momentum to maintain sufficient impact velocity after the bow shock.
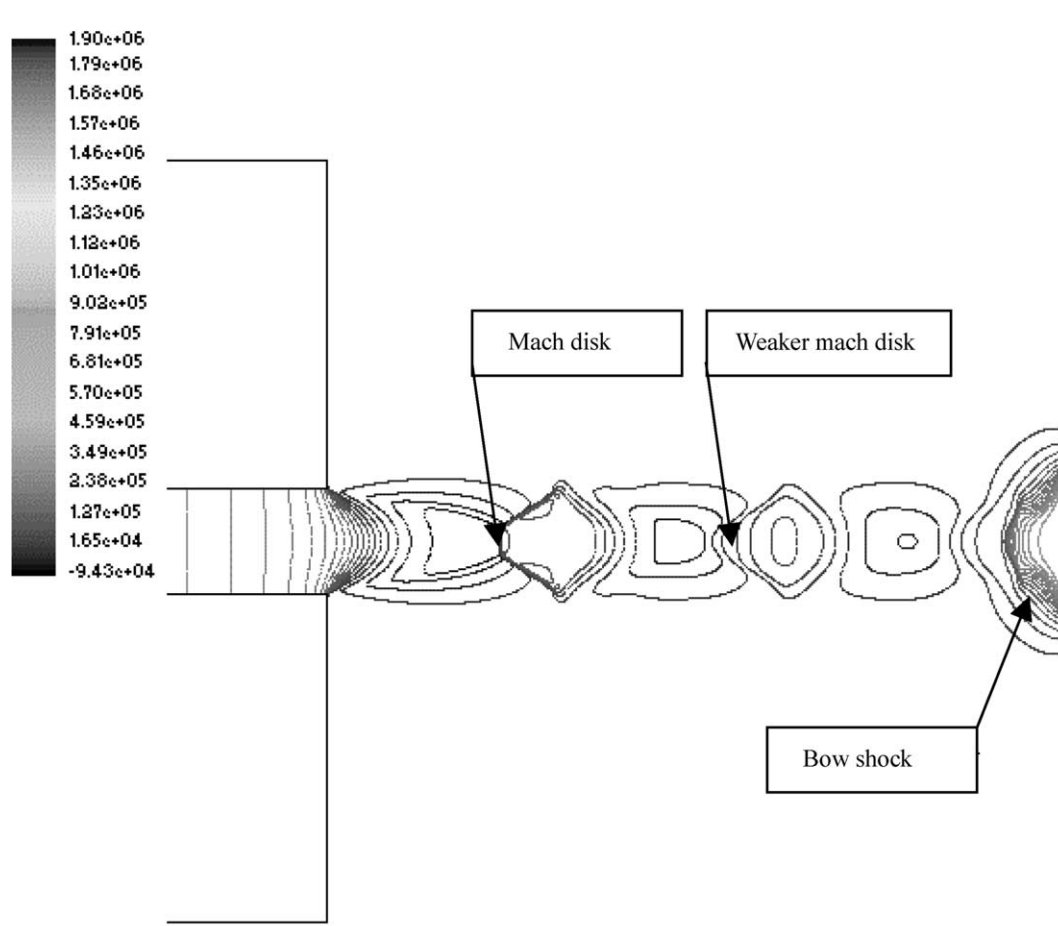

Fig. 4. The pressure contour of N_2 outside the nozzle.

However, when the particle size falls below 1 μm, the particles essentially maintain the velocity of the carrier gas [9]. The bow shock causes the small particles (or carrier gas) to decelerate to a nearly zero at the substrate. Contrary to the conventional CGDS, the smaller particles for the results here up to 20 nm in the simulation have a much larger impact velocity to 500 nm. This indicates that the inertia force is negligible for the small particles less than 1 μm while the electrostatic force becomes dominant in the ECGDS process.

Figs. 7 and 8 depict the effect of charge density on the velocity of platinum particles for particle diameters of 100 nm and 20 nm, respectively. Both figures demonstrate that when the particles move closer to the substrate, the electrostatic force gets stronger to act on the particles. The higher the particle charge densities are, the higher the particle impact velocity can be achieved. For the charge density of $9.6 \times 10^7 \, C \, m^{-3}$ (5000 elementary positive charges), the impact velocity can reach 2000 m/s for the 20 nm particles, whereas for the uncharged particles, it is essentially zero. This indicates that by using charged particles coupled with an electrostatic field in CGDS, a sufficient impact velocity can be achieved to form a coating on the substrate. Fig. 9 illustrates the comparison of velocity of 50 nm particles for three different types of materials of different density. As seen, for nano-particles the density almost has no effect on the velocity profile.
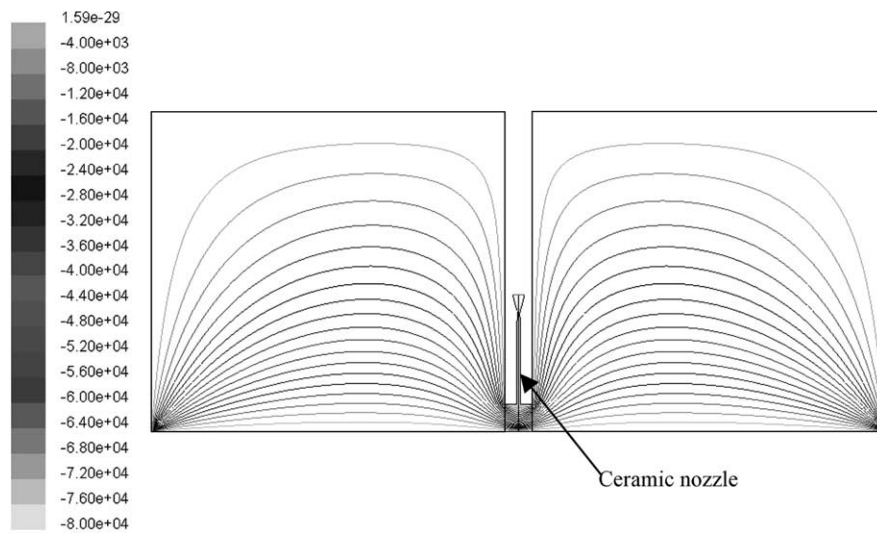

Fig. 5. Contours of electric field with high negative voltage in substrate.
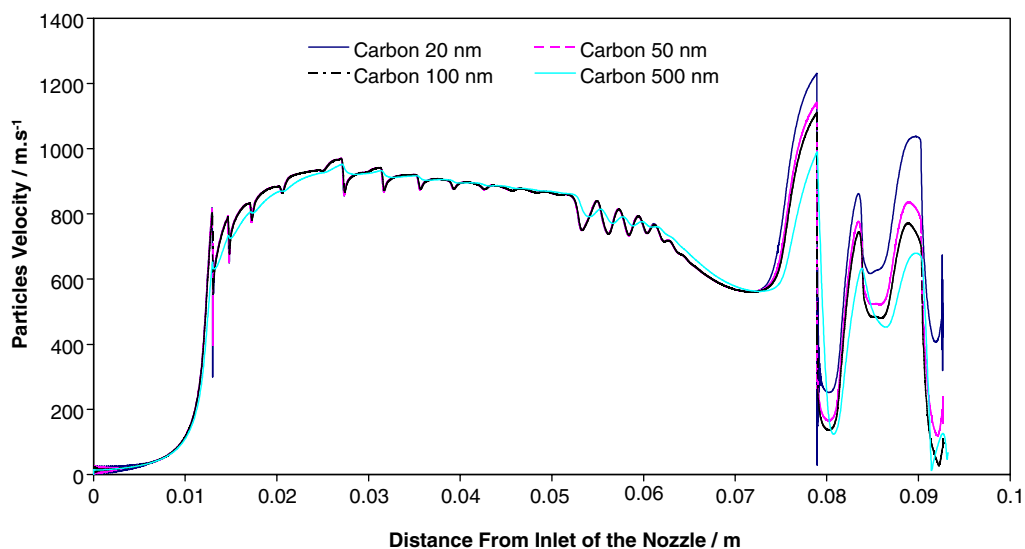

Fig. 6. The velocity of carbon particles with 1000 elementary positive charge number.
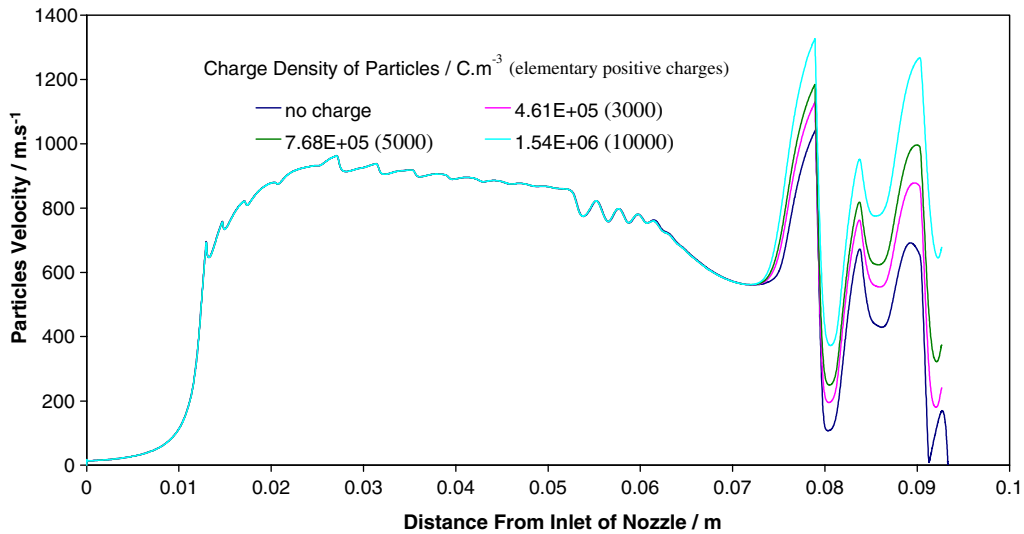
Fig. 7. The velocity of platinum particles of 100 nm diameters with various charge densities.
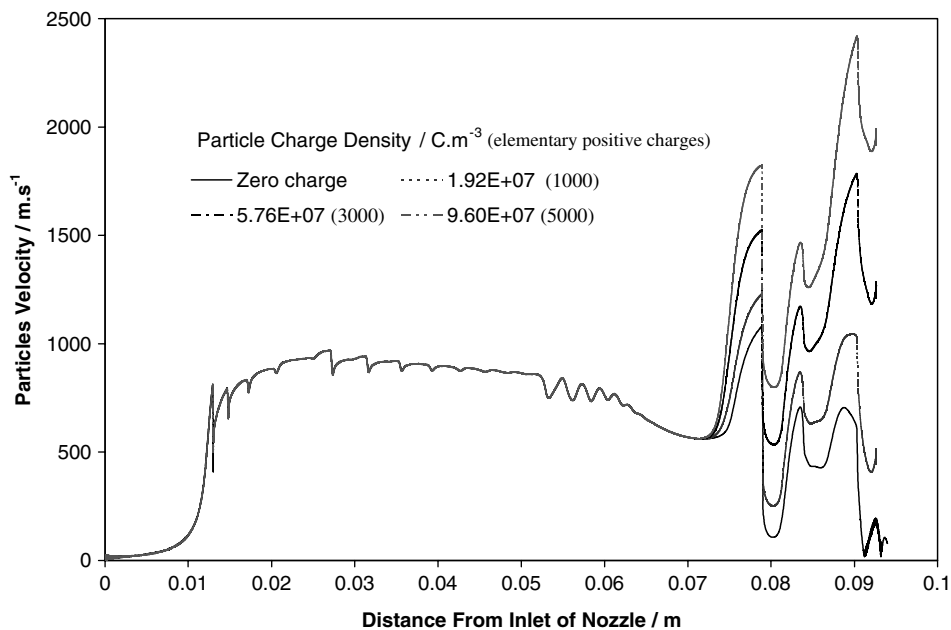

Fig. 8. The velocity of platinum particles of 20 nm diameters with various charge densities.

4. Conclusions

A numerical simulation of cold gas dynamic spraying process assisted by an electrostatic force has been conducted. The following conclusions can be drawn from the study:

1. Between the nozzle exit and the substrate, there exists a well-formed Mach disk located close to the nozzle exit, a subsequent second weaker Mach disk and a Bow shock formed on the substrate due to the under expansion of supersonic gas flow and the interaction of the supersonic jet flow with the substrate, respectively. Across the bow shock there is a steep pressure jump. The flow speed decreases to zero when the flow passes though the bow shock and approaches the substrate.

2. The maximum electric potential gradient is in the vicinity of the substrate for the static electric field.

3. The effect of the electrostatic field on the velocity distribution of carbon particles is very significant outside the nozzle. The smaller particles are the higher impact velocities on the substrate.
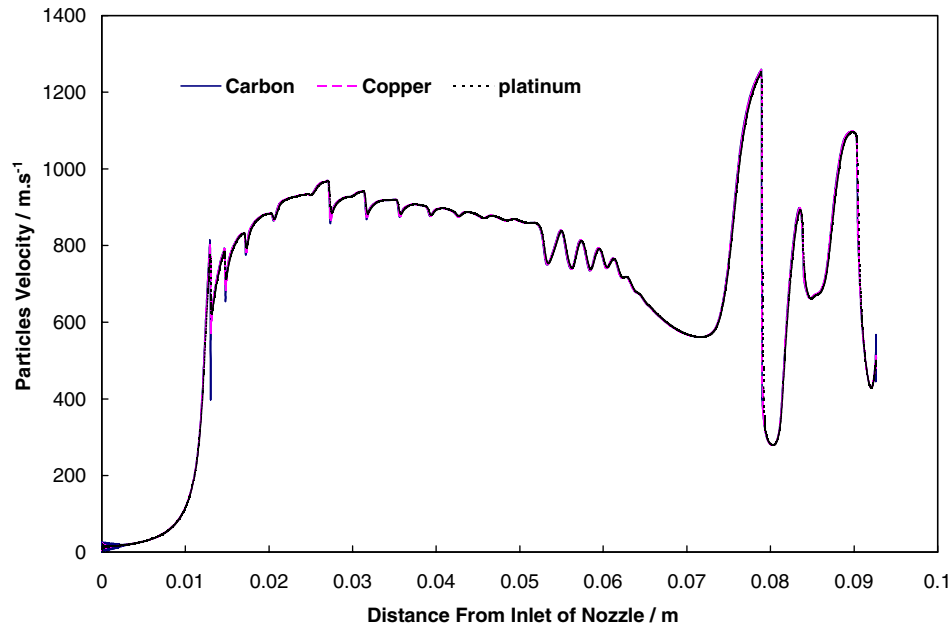
Fig. 9. The velocity of 50 nm diameters particles with different materials (3000 elementary positive charge number).

4. The higher particle impact velocity increases with the particle charge density. As the particles approach closer to the substrate, the particle electrostatic force becomes stronger.
5. For nano-particles the density has essentially no influence on the velocity profile.

Acknowledgements

References

[1] F.E. Kruis, H. Fissan, A. Peled, Synthesis of nano-particles in the gas phase for electronic, optical and magnetic applications—a review, J. Aerosol Sci. 29 (1998) 511–535.
[2] T. Junno, M.H. Magnusson, S.B. Carlsson, K. Deppert, J.-O. Malm, L. Montelius, L. Samuelson, Single-electron device via controlled assembly of designed nanoparticles, Microelectr. Eng. 47 (1999) 179–183.
[3] K.K. Likharev, Layered tunnel barriers for nonvolatile memory devices, Appl. Phys. Lett. 73 (1998) 2137–2139.
[4] T. Yoshida, Y. Yamada, T. Orii, Electroluminescence of silicon nano-crystallites prepared by pulsed laser ablation in reduced pressure inert gas, J. Appl. Phys. 83 (1998) 5427–5432.
[5] A.N. Korotkov, Wireless single-electron logic biased by alternating electric field, Appl. Phys. Lett. 6 (1995) 2412–2414.
[6] M.T. Björk, B.J. Ohlsson, T. Sass, A.I. Persson, C. Thelander, M.H. Magnusson, K. Deppert, L.R. Wallenberg, L. Samuelson, One-dimensional steeplechase for electrons realized, Nano Letters 2 (2002) 87–89.
[7] R.C. McCune, A.N. Papyrin, J.N. Hall, W.L. Riggs, P.H. Zajchowski, An exploration of the cold gas dynamic spray method for several materials systems, in: Proceedings of the 8th National Thermal Spray Conference, Houston, Texas, 1995, pp. 1–5.
[8] T.C. Jen, L.J. Li, Q.H. Chen, The acceleration of micro- and nano-particles in supersonic de-Laval-type nozzle, in: Proceedings of IMECE'03, IMECE2003-42583.
[9] T.C. Jen, L.J. Li, W.Z. Cui, Q.H. Chen, M.X. Zhang, Numerical investigations on cold gas dynamic spray process with nano- and micro- size particles, Int. J. Heat Mass Transfer 48 (2005) 4384–4396.
[10] S. Sarkar, L. Balakrishnan, Application of a reynolds-stress turbulence model to the compressible shear layer. ICASE Report 90-18, NASA CR 182002, 1990.
[11] Q. Ye, T. Steigleder, A. Scheibe, J. Domnick, Numerical simulation of the electrostatic powder coating process with a corona spraygun, J. Electrostatics 54 (2002) 189–205.